

Article

Comprehensive Properties of a Novel Quaternary Sn-Bi-Sb-Ag Solder: Wettability, Interfacial Structure and Mechanical Properties

Kaipeng Wang, Fengjiang Wang * , Ying Huang and Kai Qi

School of Materials Science and Engineering, Jiangsu University of Science and Technology, Zhenjiang 212003, China

* Correspondence: fjiangwang@just.edu.cn; Tel.: +86-511-8440-1184

Received: 25 June 2019; Accepted: 15 July 2019; Published: 17 July 2019



Abstract: Sn-58Bi eutectic solder is the most recommended low temperature Pb-free solder but is also limited from the interfacial embrittlement of Bi segregation. Since the quaternary Sn-38Bi-1.5Sb-0.7Ag solder provides a similar melting point as Sn-58Bi eutectic, this paper systematically investigated the properties of this solder from wettability, bulk tensile properties, interfacial microstructure in solder joints with a Cu substrate, interfacial evolution in joints during isothermal aging and the shear strength on ball solder joints with effect of aging conditions. The results were also compared with Sn-58Bi solder. The wettability of solder alloys was evaluated with wetting balance testing, and the quaternary Sn-38Bi-1.5Sb-0.7Ag solder had a better wettability than Sn-58Bi solder on the wetting time. Tensile tests on bulk solder alloys indicated that the quaternary Sn-38Bi-1.5Sb-0.7Ag solder had a higher tensile strength and similar elongation compared with Sn-58Bi solder due to the finely distributed SnSb and Ag₃Sn intermetallics in the solder matrix. The tensile strength of solder decreased with a decrease in the strain rate and with an increase in temperature, while the elongation of solder was independent of the temperature and strain rate. When soldering with a Cu substrate, a thin Cu₆Sn₅ intermetallic compound (IMC) is produced at the interface in the solder joint. Measurement on IMC thickness showed that the quaternary Sn-38Bi-1.5Sb-0.7Ag had a lower IMC growth rate during the following isothermal aging. Ball shear test on solder joints illustrated that the quaternary Sn-38Bi-1.5Sb-0.7Ag solder joints had higher shear strength than Sn-58Bi solder joints. Compared with the serious deterioration on shear strength of Sn-58Bi joints from isothermal aging, the quaternary Sn-38Bi-1.5Sb-0.7Ag solder joints presented a superior high temperature stability. Therefore, the quaternary Sn-38Bi-1.5Sb-0.7Ag solder provides better performances and the possibility to replace Sn-58Bi solder to realize low temperature soldering.

Keywords: Sn-Bi solder; wettability; tensile strength; interfacial IMC growth; ball shear strength; failure mode

1. Introduction

The increasing functionality and trend towards miniaturization of personal electronic devices has driven the need for smaller and thinner components, which inversely exerts a considerable challenge to the electronic assembly industry. To realize the assembling between components and the printed circuit board (PCB), Sn-based solder is the most used interconnected material. In recent years, with the implementation of RoHS (Restriction of Hazardous Substances) legislation, Sn-based Pb-free solder has gradually replaced the traditional Sn-Pb solder. Among all the developed Pb-free solders, Sn-Ag-Cu series have the most application because they provide superior mechanical performances, wettability and reliability [1,2]. However, the higher temperature required for Sn-Ag-Cu Pb-free assembling,

usually above 245 °C, promotes thermal warpage on a PCB and thinner components [3]. Therefore, the development of low temperature solder provides a lower processing temperature, and therefore reduces the thermal damage caused from using high-temperature solders. Currently, the developed low-temperature solders are mainly selected from the Sn-Bi, Sn-In or Sn-Zn series [4]; but Sn-Bi solder provides the most potential due to its low cost and better comprehensive properties [5].

The Sn-Bi binary solder system can reach the low eutectic temperature at 138 °C with a composition of Sn-58Bi, which provides the ideal processing temperature. However, there still exists some serious concerns on the application of Sn-58Bi eutectic solder, such as the interfacial embrittlement in solder joints [6–9], poorer drop reliability [10], the deterioration on joint strength after aging service [11], etc. All these problems are mainly attributed to the inherent embrittlement of Bi atoms. To improve the properties of Sn-Bi solder, many researchers have tried to decrease Bi content or incorporate additional alloying elements. In the case of decreasing Bi content in Sn-Bi solder, Shen et al. [12–14] investigated the creep and tensile properties of Sn-Bi solder with different Bi content and the interfacial reactions between solder and Cu. One of the most promising Sn-Bi solder with low Bi content is Sn-35Bi-1Ag alloy because it possesses a comparable melting point as Sn-Pb eutectic solder. The microstructure and tensile properties of solder, wetting kinetics of solder on Cu, interfacial reaction in solder joints and thermal cycling reliability were then studied [15–18]. However, Sn-35Bi-1Ag solder still exhibited lower tensile and ductility [19].

On the other hand, to improve the properties of Sn-Bi solder, many researchers tried to incorporate the alloying elements into Sn-58Bi eutectic solder. Mokhtari and Nishikawa [20] found that trace additions of Ni or In was helpful in improving the shear properties of Sn-58Bi solder joints. Sakuyama et al. [21] compared the effect of a minor addition of Ag, Cu, Zn and Sb into Sn-58Bi solder, and the results showed that the addition of Sb had the best effect on microstructural refinement and improved ductility of solder. Zhang et al. [22] recommended that the optimum content of Sb addition into Sn-Bi solder was 1.5–2.0 wt.%. Based on the Sn-Bi-Ag ternary system [23], Yan et al. [24] developed a quaternary Sn-38Bi-0.7Ag- x Sb ($x = 0.5$ – 2.5) system with the melting point ranging from 143 °C to 147 °C, and also recommended the solder with a 1.5Sb addition. Therefore, it seems the quaternary Sn-38Bi-1.5Sb-0.7Ag solder provides a lower melting temperature similar to Sn-58Bi solder while lower Bi content than Sn-58Bi solder, which inversely decreases the potentiality to produce interfacial embrittlement. However, there were less studies on this quaternary Sn-38Bi-1.5Sb-0.7Ag solder alloy. In this paper, we systematically investigated the properties of this quaternary solder from the wetting, bulk solder strength, growth behavior of intermetallic compounds (IMCs) in solder joints and shear strength of ball solder joints. To explore its potential application to replace Sn-58Bi solder, the results were also compared with Sn-58Bi eutectic solder.

2. Materials and Methods

Commercial Sn-38Bi-1.5Sb-0.7Ag and Sn-58Bi solder alloys were used in this paper. The wettability, microstructure and tensile testing were evaluated on the solder alloys.

Solder joints were prepared by reflowing solder balls on a PCB. The used PCB substrate was a FR-4 with underlying Cu pads. The thickness of the PCB, solder mask and underlying Cu pads was 1.6 mm, 35 μ m and 20 μ m, respectively. Cu pads on the PCB were defined through circular openings with diameter of 0.6 mm. Solder balls with a diameter of 0.7 mm were manufactured from bulk solder alloys. The solder balls covered with flux were then soldered on the PCB board with a peak temperature of 180 °C and a time of about 60 s. To investigate the effect of isothermal aging, ball solder joints were then aged at the temperature of 125 °C with aging times for 10, 20, 30 and 40 days, respectively. The interfacial structure and shear strength of the ball solder joints were studied.

Wettability—The wettability of solder was evaluated by the wetting balance test with standard of IPC-TM-650. A Cu sheet covered with soldering flux was dipped into the molten solder. The wetting balance curve on the relationship between the wetting force and dipped time was automatically recorded during the operation. Afterwards, zero crossing time and maximum wetting force were calculated

from the wetting curve. Commonly, a shorter time or greater force represents a better wettability for solder. The detailed testing procedure can be referenced from [25,26]. The effect of different solder temperatures and type of soldering flux was considered in this paper. The solder temperatures were set at 160, 180 and 200 °C, respectively. Two different types of soldering fluxes, commercial halide-free alcohol-based rosin-free type (IF2005C, Interflux® Electronics NV, Gent, Belgium) and water-based VOC-free (Volatile Organic Compounds) type (PacIFic 2009MLF, Interflux® Electronics NV, Gent, Belgium) were used.

Bulk tensile properties—Solder was re-melted and casted with a graphite crucible mold. To study the tensile properties of bulk solder, a dumbbell shape specimen with a gauge length of 6 mm, width of 2 mm and thickness of 2 mm was used. The test temperature ranged from 25–85 °C and the loading rate ranged from 20–60 mm/min.

Interfacial observation in solder joints—The ball solder joint was cross-sectioned and polished to a 0.05 µm surface finish with colloidal silica solution. The interfacial structure in solder joint was then observed with scanning electron microscopy (SEM) (JSM-6480, JEOL, Tokyo, Japan), and the phase composition was detected with energy dispersive spectrometer (EDS) (JEOL, Tokyo, Japan). The thickness of IMC layer was calculated from SEM images.

Shear strength on solder joints—Ball shear test was performed on the solder joint with standard of JEDEC (Solid State Technology Association) JESD22-B117A-2006. It was finished at a crosshead speed of 0.1 mm/s and a shear height of 20 µm. For each condition, the shear force was averaged from tests on 20 solder balls. The fracture morphology was observed using SEM, and the elemental analysis was performed using EDS.

3. Results and Discussion

3.1. Wettability

Wettability is very important for a solder alloy because it will influence the solderability between solder and PCB or electronic components. The most used method to evaluate the wettability of solder is the wetting balance test. During the test, a Cu plate is vertically dipped with the proper speed and depth into solder remaining at a constant temperature, and the wetting force contributes from the interaction between the surface tension and buoyancy [27]. Figure 1 shows the typical wetting curve from the wetting balance test reflecting the wetting force as a function of the immersed time.

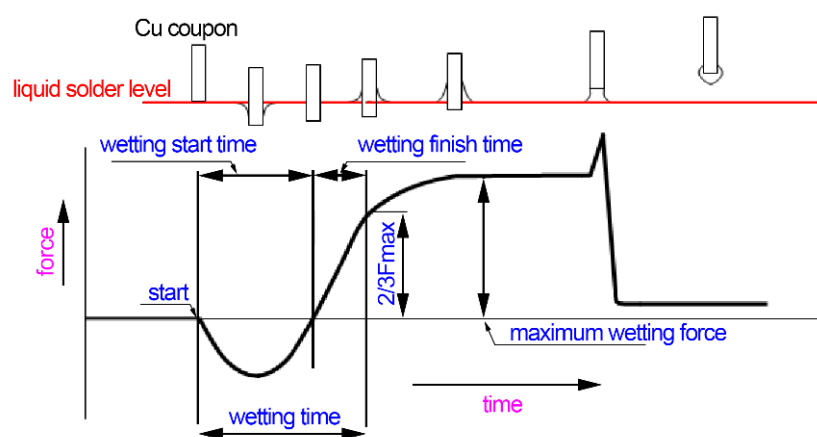


Figure 1. Schematic diagram of a typical wetting curve reflects the function between force and time.

During the wetting process, the wetting balance is commonly dominated by the surface tensions among the flux, molten solder and Cu sheet with the Young–Dupre equation [28]:

$$\cos \theta = (\gamma_{SF} - \gamma_{SL}) / \gamma_{LF} \quad (1)$$

where θ is the instantaneous contact angle, γ_{LF} , γ_{SF} and γ_{SL} are the surface tensions between flux and liquid solder, between solid Cu and flux and between solid Cu and liquid solder, respectively. Moreover, the wetting force (F) during wetting balance test is expressed as follows [28]:

$$F = \gamma_{LF} \times \cos \theta \times L - \rho V g \quad (2)$$

where L is the liquid meniscus perimeter around the immersed Cu sheet, ρ is the density of molten solder, V is the volume of the immersed Cu sheet in molten solder, and g is the acceleration of gravity. The two terms in Equation (2) represent the meniscus force and buoyancy force, respectively.

There are two important parameters to evaluate the wettability of solder: wetting start time and maximum wetting force. The wetting start time is also named as zero cross time which is defined by the period for the measured wetting force to be returned to a zero value. It reflects the time from non-wetting to wetting of molten solder on Cu under the effect of soldering flux. While, the maximum wetting force is produced when the immersion depth of the Cu sheet is stabilized in molten solder and the meniscus force reaches the maximum. Commonly, the shorter the wetting start time or the higher the maximum wetting force, the higher wettability of solder.

The wetting start time and maximum wetting force are plotted in Figure 2, in which SBSA and SB represent Sn-38Bi-1.5Sb-0.7Ag and Sn-58Bi solder, respectively. Three temperatures of 160, 180 and 200 °C were selected to study the effect of solder temperature, and the halide-free alcohol-based flux and water-based flux were used to investigate the effect of the type of soldering flux. In Figure 2a, it can be found there is a shorter wetting time for Sn-38Bi-1.5Sb-0.7Ag solder compared with Sn-58Bi solder, which is independent of the soldering flux and solder temperature. Moreover, with solder temperature increasing, the wetting time decreases for these two solders. In the case of the effect of type of soldering flux, it can be found that alcohol-based flux presents a far shorter time during the wetting test. Regarding the wetting force, Sn-38Bi-1.5Sb-0.7Ag solder is a little higher than Sn-58Bi solder, while the solder temperature and soldering flux have no obvious effect on the force, as shown in Figure 2b.

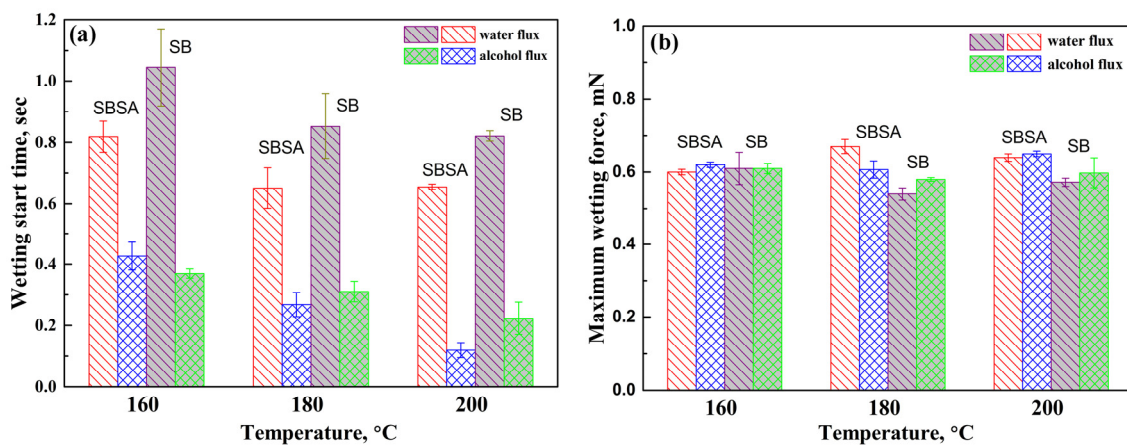


Figure 2. Comparison on the wettability of Sn-38Bi-1.5Sb-0.7Ag and Sn-58Bi solder: (a) wetting time and (b) wetting force.

Therefore, Sn-38Bi-1.5Sb-0.7Ag solder presents better wettability from the wetting time and wetting force than Sn-58Bi solder, which may be attributed to the lower Bi content and Ag addition because the Bi element was more inclined to oxidize while Ag proved to be helpful in increasing the wettability of solder [26,27]. The variation of solder temperature or soldering flux will be helpful in deciding the optimal parameters for soldering. In this paper, the elevated temperature promoted the wettability of solder especially from the wetting time because it helped to decrease the surface tension of molten solder and improve the deoxidized capability of soldering flux. Soldering flux also has an obvious effect on the wettability of solder, and the results in Figure 2 show that alcohol-based flux

presented a very good wetting time compared with water-based rosin-free flux for Sn-38Bi-1.5Sb-0.7Ag and Sn-58Bi solders. The activators in the flux were dissolved easier in the alcohol solvent than in the water, and the evaporation rate of the alcohol solvent was also higher than that of water. Correspondingly, the reaction between acid activators in the alcohol-based flux and oxide film of solder or Cu occurred in a shorter period, which induced a better wetting start time.

3.2. Interfacial Evolution in Solder Joints

During soldering condition, solder alloy will react with the metallic pad in the PCB to produce an IMC layer at the interface, which ensures the metallurgical bonding in solder joints. Afterwards, its thickness will increase with the aging condition, which will deteriorate the reliability of solder joints. Therefore, it is necessary to investigate the formation and evolution of interfacial IMC layers in Sn-38Bi-1.5Sb-0.7Ag solder joints. In this paper, the metallic pad in the PCB is the most commonly used Cu pad.

Figure 3 shows the macroscopic microstructure of the ball solder joint and magnified interfacial structure in the joint for Sn-38Bi-1.5Sb-0.7Ag and Sn-58Bi solders. The dark region is Sn-rich phases and the white region is Bi phases. In Sn-38Bi-1.5Sb-0.7Ag solder joint, large amounts of primary Sn-rich phases were produced, while Bi elements accumulated together to produce coarsened phases, as shown in Figure 3a. To obtain the distribution of Sb and Ag addition in solder, EDS was detected with the results shown in Figure 3c. Ag reacted with Sn to produce Ag_3Sn IMC particles, which were distributed in the solder matrix. According to the Sn-Sb phase diagram, Sb reacts with Sn to produce SnSb intermediate phases, which was also confirmed with the Sn-Bi-Sb system by Zhang et al. [22]. In this paper, Sb element was detected in primary Sn-rich phases from the EDS result, and therefore, SnSb phases possibly existed with Sn-rich phases. At the interface of the Sn-38Bi-1.5Sb-0.7Ag solder joint, a thin IMC layer with a thickness of about 1–2 μm was produced between solder and Cu pad, and its composition is confirmed as Cu_6Sn_5 phase in Figure 3c. Cu_6Sn_5 IMC was obtained from the reaction between Sn atoms from solder and Cu atoms from substrate, and it seems that Sb and Ag did not enroll in this reaction. In Sn-58Bi solder joints, as seen from Figure 3b, the microstructure of solder matrix belongs to a typical eutectic structure which is composed of Sn-rich and Bi phases with fine distribution. They also produced a thin IMC layer at the interface with a thickness of about 1 μm . Its composition is also Cu_6Sn_5 from our previous result on X-ray diffraction (XRD) analysis [9].

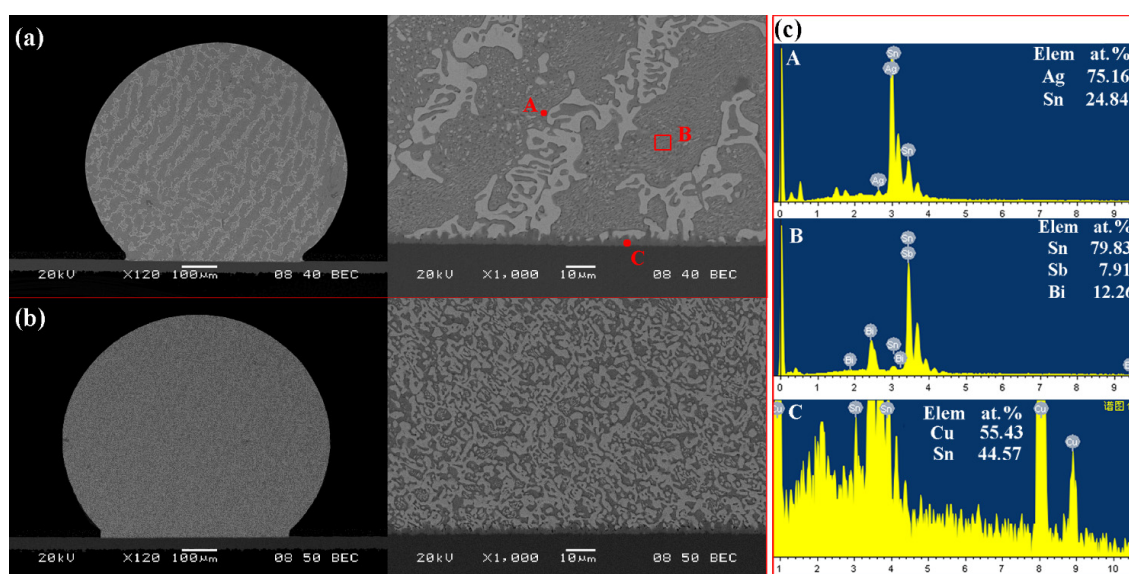


Figure 3. Microstructural observation and compositional analysis in soldered joints for (a) Sn-38Bi-1.5Sb-0.7Ag solder, (b) Sn-58Bi solder and (c) energy dispersive spectrometer (EDS) results on marked phases in Sn-38Bi-1.5Sb-0.7Ag solder joint.

Figure 4 shows the effect of isothermal aging on the solder joints at aging temperature of 125 °C with aging time ranging from 10 to 40 days. In Sn-58Bi solder joints, as shown in Figure 4b, with a prolonged aging time, the macroscopic observation shows that Sn-rich and Bi phases obviously coarsened, and interfacial evolution shows that the Cu_6Sn_5 IMC layer grew rapidly as the thickness increased from the initial 1 μm in soldering condition to about 9 μm after 40 days of aging. However, in Sn-38Bi-1.5Sb-0.7Ag ball solder joints shown in Figure 4a, high temperature aging promoted the uniform distribution of Sn-rich and Bi phases in the solder matrix but did not induce the obvious coarsening on them. The thickness of the IMC layer at the interface of Sn-38Bi-1.5Sb-0.7Ag/Cu also increased with thermal aging. However, after 40 days aging, the thickness of the IMC layer was about 7 μm , which was thinner than that in Sn-58Bi solder joint. Therefore, in contrast to Sn-58Bi solder joint, Sn-38Bi-1.5Sb-0.7Ag solder alloy could form stable grains in solder joint and effectively retard the interfacial IMC growth during isothermal aging.

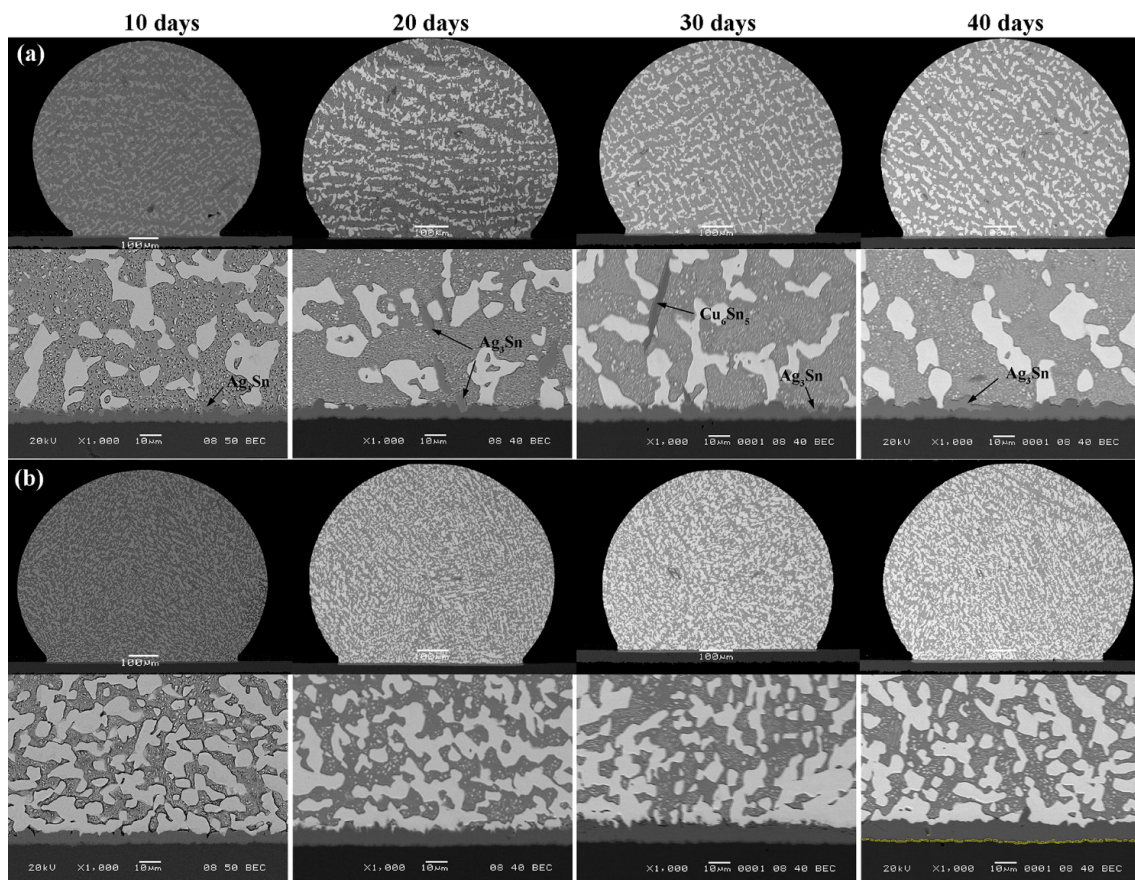


Figure 4. Microstructural evolution in solder joints during aging: (a) Sn-38Bi-1.5Sb-0.7Ag and (b) Sn-58Bi.

It is well known that the growth of an IMC layer at the interface induced from aging usually follows the parabolic law equation:

$$d = K\sqrt{t} \quad (3)$$

where d is the IMC thickness, K is the growth rate constant and t is the aging time. Therefore, the relationship between IMC thickness and square root of aging days in Sn-38Bi-1.5Sb-0.7Ag and Sn-58Bi solder joints is plotted in Figure 5, which suggests that the growth of the IMC layer at the interface was diffusion-controlled during isothermal aging. Meanwhile, Sn-38Bi-1.5Sb-0.7Ag solder joint presented a lower growth rate for interfacial IMC compared with Sn-58Bi solder joint. The depressing effect of Ag and Sb addition on IMC growth might be explained by the heterogeneous nucleation theory

because Ag or Sb was easier to react with Sn to produce Ag_3Sn or SnSb particles due to their higher affinity to Sn, which became the heterogeneous nucleation sites of Cu_6Sn_5 IMC and inhibited the IMC growth [29].

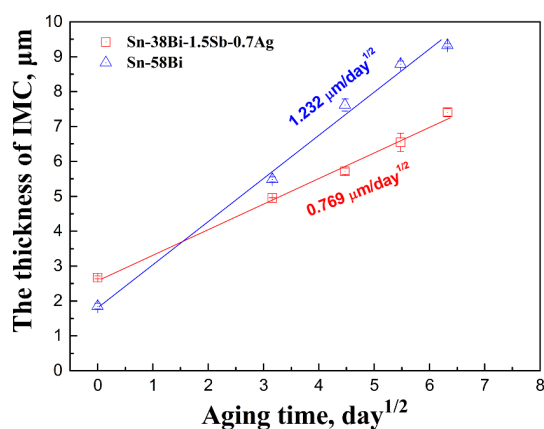


Figure 5. Relationship between the thickness of interfacial intermetallic compound (IMC) and aging duration.

3.3. Tensile Properties of Bulk Solder Alloy

Tensile testing was implemented on bulk solder alloy to decide the mechanical properties of Sn-38Bi-1.5Sb-0.7Ag and Sn-58Bi eutectic solders, and the resulting tensile strength and elongation with consideration of the loading rate and the ambient temperature are plotted in Figure 6. Regarding tensile strength, as shown in Figure 6a, Sn-38Bi-1.5Sb-0.7Ag solder always presents a higher strength than Sn-58Bi eutectic solder independent of temperature and loading rate. An increase in temperature can obviously decrease the tensile strength of solder, but an increase of the loading rate plays an ignorable effect on tensile strength. Regarding elongation of Sn-38Bi-1.5Sb-0.7Ag solder, as shown in Figure 6b, it increases with the temperature at the lower loading rate or increases with the loading rate at a lower temperature. Compared with Sn-Ag-Cu solder, this novel quaternary solder also presents a superior mechanical performance because it shows a similar elongation and a higher tensile strength [30]. However, for Sn-58Bi solder, elongation was not affected by the loading rate but increased with the temperature; particularly the elongation of Sn-58Bi reached about 150% when the temperature reached 85 °C. Figure 7 shows the corresponding relationship between the tensile curves and fracture morphologies for Sn-38Bi-1.5Sb-0.7Ag and Sn-58Bi solders tested at the loading rate of 20 mm/min. At room temperature, the tensile curves presented typical brittle characteristics without obvious plastic deformation, and the intergranular fractures were observed in the fracture morphologies. With an increase in temperature, plastic deformation occurred in the tensile curves for Sn-38Bi-1.5Sb-0.7Ag solder at 55 °C and 85 °C and for Sn-58Bi solder at 85 °C. Accordingly, many dimples were observed in these fractures, which represent the ductile fractures.

The microstructure of Sn-38Bi-1.5Sb-0.7Ag solder was mainly composed of β -Sn and Bi-rich phases with uniformly distributed Ag_3Sn and SnSb intermediate phases which improved the mechanical properties of solder. Furthermore, it is well known that Bi possesses the superplastic effect [31], and therefore Sn-58Bi solder shows a superior elongation value at the temperature of 85 °C due to its higher Bi content in solder.

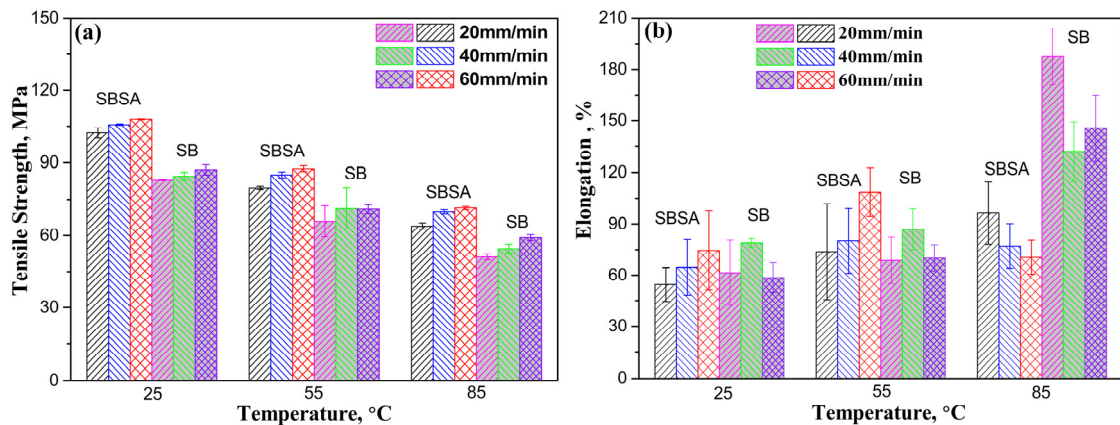


Figure 6. Relationship between the tensile strength/the elongation and the loading rate/the ambient temperature. (a) the tensile strength; (b) the elongation.

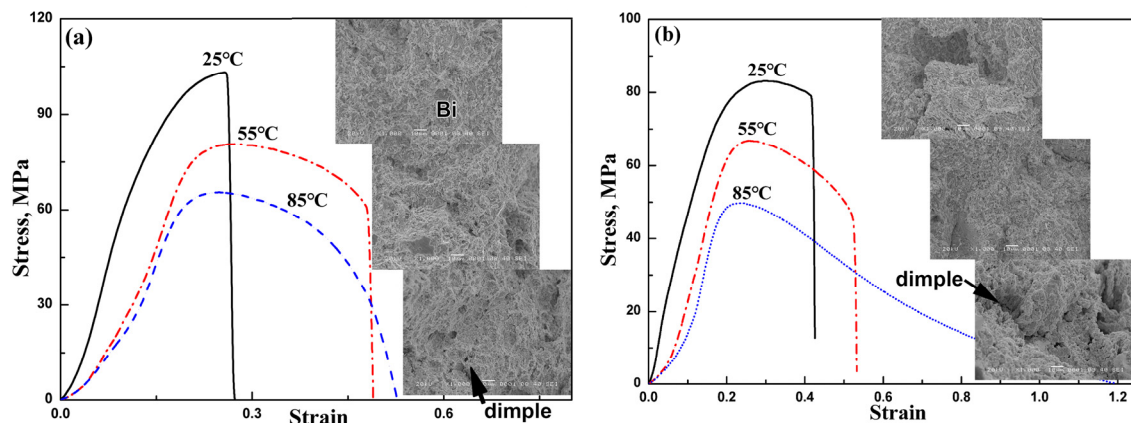


Figure 7. Fracture analysis with the relationship between tensile curves and fracture morphologies: (a) Sn-38Bi-1.5Sb-0.7Ag and (b) Sn-58Bi.

3.4. Mechanical Properties of Solder Joints

Mechanical properties of solder joints were evaluated with the ball shear test. Figure 8a shows an example of shear curves for Sn-38Bi-1.5Sb-0.7Ag and Sn-58Bi solder joints with soldering condition and 40 days aging condition, respectively. From the shear curves, we can obtain the maximum shear force, fracture initiation energy and fracture propagation energy. The transition point from initial energy to propagation energy was decided by the maximum strength [32]. Comparison on the shear force between Sn-38Bi-1.5Sb-0.7Ag and Sn-58Bi solder joints after aging is plotted in Figure 8b. During soldering condition, the Sn-38Bi-1.5Sb-0.7Ag solder joint had the average shear strength of approximately 19.5 N, which was higher than Sn-58Bi as-soldered joint. After 40 days aging, the average shear strength of Sn-38Bi-1.5Sb-0.7Ag and Sn-58Bi solder joints was about 20 N and 15 N, respectively. Therefore, annealing at a higher temperature would not affect Sn-38Bi-1.5Sb-0.7Ag solder joint, but obviously deteriorated the mechanical performance of Sn-58Bi solder joint. Figure 8c shows the total shear energy, fracture initiation energy and fracture propagation energy of the solder joint samples at 0, 10, 20, 30 and 40 days of aging. Total shear energy was defined as the combination of fracture initiation and fracture propagation energy. Sn-38Bi-1.5Sb-0.7Ag resulted in a higher shear energy value compared to Sn-58Bi. It was observed that with an increased aging time, the total shear energy of Sn-38Bi-1.5Sb-0.7Ag joint increased firstly and then decreased, while Sn-58Bi joint always displayed a decrease in shear energy value after aging. On the other hand, by distinguishing the fracture initiation and propagation energy, the relative energy required for a solder joint fracture to initiate and propagate could be determined. As shown in Figure 8c, fracture initiation energy of solder joints had a similar trend to the total shear energy. For Sn-38Bi-1.5Sb-0.7Ag as-soldered joint,

approximately 2.00 mJ is required to initiate a solder joint fracture. It increases after aging time of 20 days to approximately 2.34 mJ, and then decreases after aging time of 40 days to approximately 2.05 mJ. From the fracture propagation energy, Sn-58Bi as-soldered joint resulted in a higher value compared to Sn-38Bi-1.5Sb-0.7Ag solder joints, but no obvious change in fracture propagation energy in Sn-58Bi solder joints after aging occurred. However, for Sn-38Bi-1.5Sb-0.7Ag, fracture propagation energy of solder joints had a similar trend to the total fracture initiation energy.

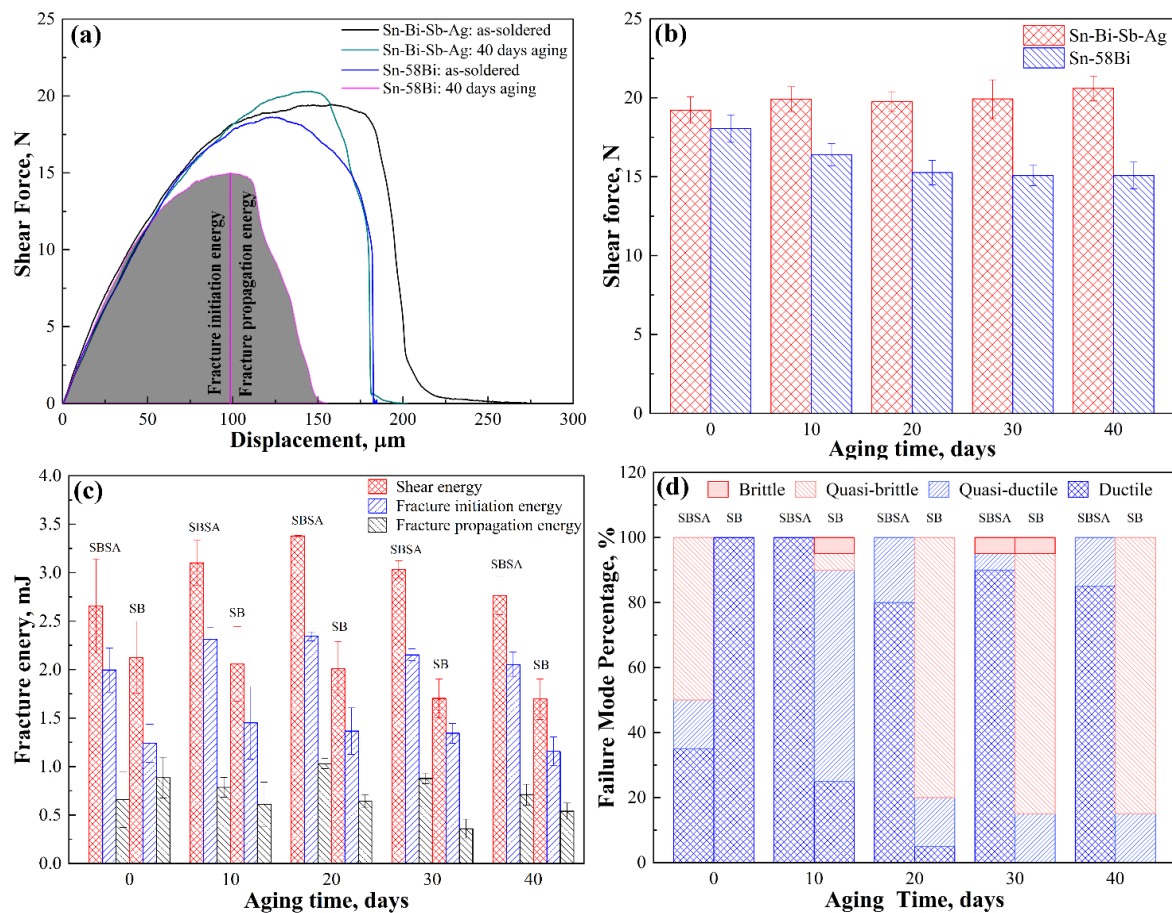


Figure 8. (a) Shear force versus displacement curves with the definition of fracture energy, (b) shear strength, (c) fracture energy and (d) fracture mode distribution of ball shear tests on as-soldered and as-aged solder joints.

In fact, the shear energy also reflects the ductile or brittle failure during ball shear tests, which is related with the strength of bulk solder and the strength of interfacial adhesive strength. Figure 9 shows the SEM images on fracture morphologies of Sn-38Bi-1.5Sb-0.7Ag and Sn-58Bi solder joints with as-soldered, 20 days aging and 40 days aging conditions. Sn-38Bi-1.5Sb-0.7Ag solder joints exhibited ductile characteristics with fracture mainly occurring in solder matrix while Sn-58Bi solder joints were fractured in the solder matrix in as-soldered state but were fractured at the interface after aging. From the fracture morphologies, there usually exists four different failure modes: ductile (100% in solder matrix), quasi-ductile (>50% area with bulk solder), quasi-brittle (>50% area with exposed interfacial layer) and brittle (100% area with exposed interfacial layer) [32,33]. Figure 10 shows a typical brittle fracture mode on the elemental mapping of Sn-58Bi solder joint after aging for 40 days, in which the fracture surface was mainly composed of Cu and Sn atoms. Figure 8d shows the fracture mode distribution of the solder joint collected from SEM images on 20 samples. On as-reflowed solder joints, it is observed that Sn-38Bi-1.5Sb-0.7Ag solder joints had half of the quasi-brittle fracture, while 100% of samples experienced ductile failure in Sn-58Bi solder joints. During aging condition, most of the

Sn-38Bi-1.5Sb-0.7Ag solder joints experienced ductile fracture and a small percentage of quasi-ductile failure was observed. However, a small percentage of brittle and quasi-brittle failure was observed in Sn-58Bi solder joints after aging for 10 days, while the majority of the fracture modes were relatively brittle with aging time increasing.

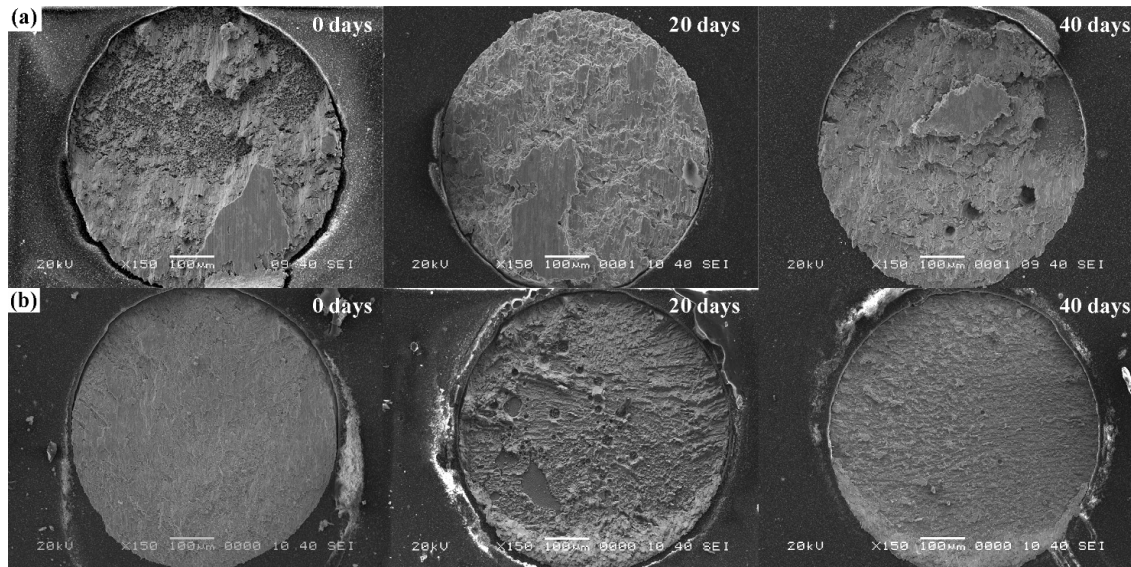


Figure 9. Fracture morphologies in (a) Sn-38Bi-1.5Sb-0.7Ag and (b) Sn-58Bi solder joints.

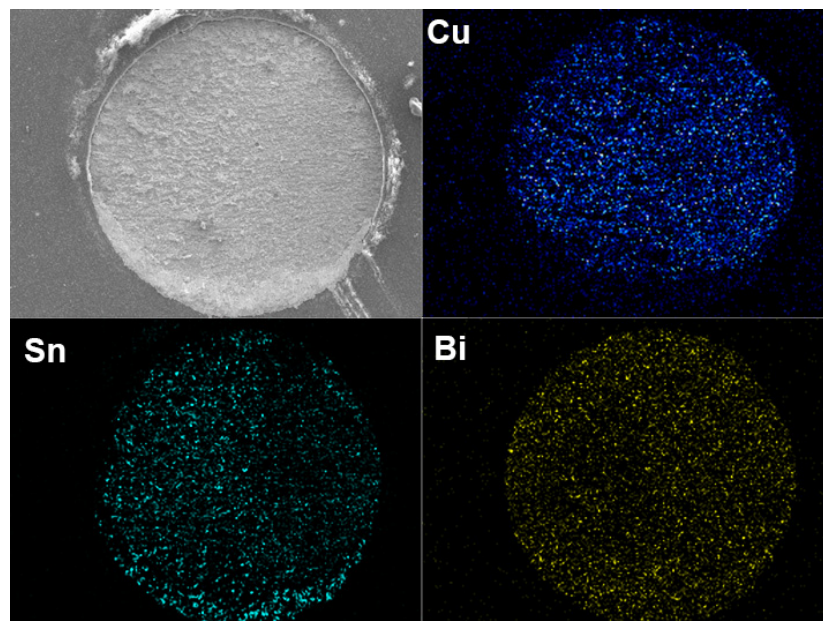


Figure 10. Illustration on a typical brittle fracture mode with the elemental mapping of Sn-58Bi joint after aging for 40 days.

The fracture mode was mainly decided by the strength of bulk solder matrix and interfacial adhesive strength. If the solder strength was higher than IMC strength, the fracture would occur along the interfacial area to produce a quasi-brittle or brittle failure mode, or else, the fracture would occur in the solder matrix in a ductile or quasi-ductile mode. In Sn-38Bi-1.5Sb-0.7Ag solder joints, the solder strength was higher than the interfacial adhesive strength in Sn-38Bi-1.5Sb-0.7Ag as-soldered joint due to the existence of Ag_3Sn and SnSb phases, and accordingly the quasi-brittle or brittle mode occurred with the fracture mainly propagating along the interface. After isothermal aging, the higher

solder strength and thinner IMC layer during aging condition promoted a higher joint shear strength with fracture in the solder matrix. In Sn-58Bi solder joints, the over growth of interfacial IMC and the existence of interfacial Bi-rich layer seriously deteriorated the joint performance [34,35].

4. Conclusions

Since Sn-38Bi-1.5Sb-0.7Ag quaternary solder provides a similar melting point as Sn-58Bi, this paper aimed to explore the possibility of using it to replace the currently used eutectic Sn-58Bi solder. The wettability of solder, mechanical properties of bulk solder alloy, formation and the interfacial evolution in solder joints and mechanical properties of solder joints were compared between Sn-38Bi-1.5Sb-0.7Ag and Sn-58Bi solder. The main achievements can be listed as follows:

- (1) Wetting balance tests illustrated that Sn-38Bi-1.5Sb-0.7Ag solder had a better wettability on the wetting time than Sn-58Bi solder.
- (2) Compared with Sn-58Bi solder, Sn-38Bi-1.5Sb-0.7Ag bulk solder had a higher tensile strength and a similar elongation. The tensile strength increased while the elongation of solder decreased with testing temperature.
- (3) In solder/Cu joints, the IMC growth rate in Sn-38Bi-1.5Sb-0.7Ag solder joints was slower than that in Sn-58Bi eutectic joints during isothermal aging.
- (4) Ball shear tests illustrated that Sn-38Bi-1.5Sb-0.7Ag solder joints had a higher shear strength than Sn-58Bi solder joints after isothermal aging.

Author Contributions: Experimental design, F.W. and K.Q.; wettability, K.W.; interfacial observation, Y.H.; Mechanical tests, K.W. and Y.H.; writing—original draft preparation, K.W.; writing—review and editing, F.W.

Funding: This research was funded by the National Natural Science Foundation of China, grant number 51875269.

Conflicts of Interest: The authors declare no conflict of interest.

References

1. Shnawah, D.A.; Sabri, M.F.M.; Badruddin, I.A. A review on thermal cycling and drop impact reliability of SAC solder joint in portable electronic products. *Microelectron. Reliab.* **2012**, *52*, 90–99. [[CrossRef](#)]
2. Ma, H.; Suhling, J.C. A review of mechanical properties of lead-free solders for electronic packaging. *J. Mater. Sci.* **2009**, *44*, 1141–1158. [[CrossRef](#)]
3. Sidhu, R.S.; Aspandiar, R.; Vandervoort, S.; Amir, D.; Murtagian, G. Impact of processing conditions and solder materials on surface mount assembly defects. *JOM* **2011**, *63*, 47–51. [[CrossRef](#)]
4. Kotadia, H.R.; Howes, P.D.; Mannan, S.H. A review: On the development of low melting temperature Pb-free solders. *Microelectron. Reliab.* **2014**, *54*, 1253–1273. [[CrossRef](#)]
5. Wang, F.; Chen, H.; Huang, Y.; Liu, L.; Zhang, Z. Recent progress on the development of Sn–Bi based low-temperature Pb-free solders. *J. Mater. Sci.: Mater. Electron.* **2019**, *30*, 3222–3243. [[CrossRef](#)]
6. Zou, H.F.; Zhang, Q.K.; Zhang, Z.F. Transition of Bi embrittlement of SnBi/Cu joint couples with reflow temperature. *J. Mater. Res.* **2011**, *26*, 449–454. [[CrossRef](#)]
7. Chi, C.C.; Tsao, C.W.; Chuang, T.H. Intermetallic reactions in reflowed and aged Sn-58Bi BGA packages with Au/Ni/Cu pads. *J. Mater. Eng. Perform.* **2007**, *17*, 134–140. [[CrossRef](#)]
8. Li, J.F.; Mannan, S.H.; Clode, M.P.; Chen, K.; Whalley, D.C.; Liu, C.; Hutt, D.A. Comparison of interfacial reactions of Ni and Ni-P in extended contact with liquid Sn-Bi-based solders. *Acta Mater.* **2007**, *55*, 737–752. [[CrossRef](#)]
9. Wang, F.; Zhou, L.; Wang, X.; He, P. Microstructural evolution and joint strength of Sn-58Bi/Cu joints through minor Zn alloying substrate during isothermal aging. *J. Alloys Compd.* **2016**, *688*, 639–648. [[CrossRef](#)]
10. Myung, W.-R.; Kim, Y.; Kim, K.-Y.; Jung, S.-B. Drop reliability of Epoxy-contained Sn-58 wt.%Bi solder joint with ENIG and ENEPIG surface finish under temperature and humidity test. *J. Electron. Mater.* **2016**, *45*, 3651–3658. [[CrossRef](#)]
11. Yu, X.; Hu, X.; Li, Y.; Liu, T.; Zhang, R.; Min, Z. Tensile properties of Cu/Sn-58Bi/Cu soldered joints subjected to isothermal aging. *J. Mater. Sci.: Mater. Electron.* **2014**, *25*, 2416–2425. [[CrossRef](#)]

12. Lai, Z.; Ye, D. Microstructure and fracture behavior of non eutectic Sn–Bi solder alloys. *J. Mater. Sci.: Mater. Electron.* **2016**, *27*, 3182–3192. [[CrossRef](#)]
13. Wang, F.; Huang, Y.; Zhang, Z.; Yan, C. Interfacial reaction and mechanical properties of Sn–Bi solder joints. *Materials* **2017**, *10*, 920. [[CrossRef](#)] [[PubMed](#)]
14. Shen, L.; Septiawandani, P.; Chen, Z. Elastic modulus, hardness and creep performance of SnBi alloys using nanoindentation. *Mater. Sci. Eng. A* **2012**, *558*, 253–258. [[CrossRef](#)]
15. Li, Y.; Wang, Z.; Long, W.; Lei, M.; Hu, X. Wetting kinetics and spreading phenomena of Sn–35Bi–1Ag solder on different substrates. *J. Mater. Sci.: Mater. Electron.* **2018**, *29*, 13914–13924. [[CrossRef](#)]
16. Gain, A.K.; Zhang, L. Effect of thin gold/nickel coating on the microstructure, wettability and hardness of lead-free tin–bismuth–silver solder. *J. Mater. Sci.: Mater. Electron.* **2017**, *28*, 4885–4896. [[CrossRef](#)]
17. Fouzder, T.; Gain, A.K.; Chan, D.K. Microstructure, wetting characteristics and hardness of tin–bismuth–silver (Sn–Bi–Ag) solders on silver (Ag)-surface finished copper (Cu) substrates. *J. Mater. Sci.: Mater. Electron.* **2017**, *28*, 16921–16931. [[CrossRef](#)]
18. Zhang, L.; Sun, L.; Guo, Y.-h. Microstructures and properties of Sn58Bi, Sn35Bi0.3Ag, Sn35Bi1.0Ag solder and solder joints. *J. Mater. Sci.: Mater. Electron.* **2015**, *26*, 7629–7634. [[CrossRef](#)]
19. Silva, B.L.; Xavier, M.G.C.; Garcia, A.; Spinelli, J.E. Cu and Ag additions affecting the solidification microstructure and tensile properties of Sn–Bi lead-free solder alloys. *Mater. Sci. Eng. A* **2017**, *705*, 325–334. [[CrossRef](#)]
20. Mokhtari, O.; Nishikawa, H. Correlation between microstructure and mechanical properties of Sn–Bi–X solders. *Mater. Sci. Eng. A* **2016**, *651*, 831–839. [[CrossRef](#)]
21. Sakuyama, S.; Akamatsu, T.; Uenishi, K.; Sato, T. Effects of a third element on microstructure and mechanical properties of eutectic Sn–Bi solder. *Trans. Jpn. Inst. Electron. Packag.* **2009**, *2*, 98–103. [[CrossRef](#)]
22. Zhang, C.; Liu, S.-d.; Qian, G.-t.; Zhou, J.; Xue, F. Effect of Sb content on properties of Sn–Bi solders. *Trans. Nonferrous Met. Soc. China* **2014**, *24*, 184–191. [[CrossRef](#)]
23. Kattner, U.; Boettinger, W.J. On the Sn–Bi–Ag ternary phase diagram. *J. Electron. Mater.* **1994**, *23*, 603–610. [[CrossRef](#)]
24. Yan, J.K.; Xu, F.X.; Chen, D.D.; Teng, Y.; Gan, Y.W. A study on microstructure and properties of quaternary SnBiAgSb solder alloy. *J. Kunming Univ. Sci. Technol.* **2018**, *43*, 22–27.
25. Hasnine, M. Effects of In and Sb addition on the thermal and wetting behavior of Sn–3.5Ag solder. *Solder Surf. Mt. Technol.* **2018**, *30*, 233–240. [[CrossRef](#)]
26. Jung, D.-H.; Jung, J.-P. Review of the wettability of solder with a wetting balance test for recent advanced microelectronic packaging. *Crit. Rev. Solid State Mater. Sci.* **2018**, *43*, 1–20. [[CrossRef](#)]
27. Noor, E.E.M.; Nasir, N.F.M.; Idris, S.R.A. A review: Lead free solder and its wettability properties. *Solder Surf. Mt. Technol.* **2016**, *28*, 125–132. [[CrossRef](#)]
28. Martorano, K.M.; Martorano, M.A.; Brandi, S.D. Optimal conditions for the wetting balance test. *J. Mater. Process. Technol.* **2009**, *209*, 3089–3095. [[CrossRef](#)]
29. Chen, B.L.; Li, G.Y. Influence of Sb on IMC growth in Sn–Ag–Cu–Sb Pb-free solder joints in reflow process. *Thin Solid Films* **2004**, *462*, 395–401. [[CrossRef](#)]
30. Che, F.X.; Zhu, W.H.; Poh, E.S.W.; Zhang, X.W.; Zhang, X.R. The study of mechanical properties of Sn–Ag–Cu lead-free solders with different Ag contents and Ni doping under different strain rates and temperatures. *J. Alloys Compd.* **2010**, *507*, 215–224. [[CrossRef](#)]
31. Alden, T.H. The origin of superplasticity in the Sn–5%Bi alloy. *Acta Metall.* **1967**, *15*, 469–480. [[CrossRef](#)]
32. Salleh, M.A.A.M.; McDonald, S.D.; Nogita, K. Effects of Ni and TiO₂ additions in as-reflowed and annealed Sn0.7Cu solders on Cu substrates. *J. Mater. Process. Technol.* **2017**, *242*, 235–245. [[CrossRef](#)]
33. Wang, F.J.; Chen, H.; Huang, Y.; Yan, C. Interfacial behavior and joint strength of Sn–Bi solder with solid solution compositions. *J. Mater. Sci.: Mater. Electron.* **2018**, *29*, 11409–11420. [[CrossRef](#)]
34. Wang, F.; Li, D.; Zhang, Z.; Wu, M.; Yan, C. Improvement on interfacial structure and properties of Sn–58Bi/Cu joint using Sn–3.0Ag–0.5Cu solder as barrier. *J. Mater. Sci.: Mater. Electron.* **2017**, *28*, 19051–19060. [[CrossRef](#)]
35. Zhang, Q.K.; Zou, H.F.; Zhang, Z.F. Influences of substrate alloying and reflow temperature on Bi segregation behaviors at Sn–Bi/Cu interface. *J. Electron. Mater.* **2011**, *40*, 2320–2328. [[CrossRef](#)]

